J Mater Sci (2009) 44:3265–3272
DOI 10.1007/s10853-009-3438-3

Comparison of the coatings deposited using Ti and B_4C powder by reactive plasma spraying in air and low pressure

Zhengping Mao · Jing Ma · Jun Wang · Baode Sun

Received: 18 October 2008 / Accepted: 24 March 2009 / Published online: 9 April 2009

Abstract The coatings were deposited by reactive plasma spraying (RPS) in air and low-pressure plasma spraying (LPPS) based on the reaction between Ti and B_4C powder, respectively. The thermal spray powder of Ti and B_4C added with powder Cr (metallic binder) in air is compared with that without powder Cr addition in the low pressure. (Prior to deposition, the powder was screened and separated for RPS whereas spray drying, sintering and sieving were done for LPPS.) The phase composition and the microstructure of coatings were studied by X-ray diffractometer (XRD) and scanning electron microscopy (SEM). The anti-corrosion property of coatings was also investigated. It is found that the coating prepared by RPS, which is more densification, is composed of TiN, TiB_2, and a small phase fraction of titanium oxides. The composition of the coating deposited by reactive LPPS is TiB_2, Ti(C, N), Ti_4N_{3-x} and impurity phase of Ti_5Si_3. There is no appearance of titanium oxides in low pressure. The coatings have the typical lamellar structure and adhere to the bond coating well. The mean Vickers microhardness value of the coating deposited by RPS is higher than that of the coating deposited by LPPS. Furthermore, the corrosion resistance of the coating deposited by RPS is superior to that of the coating prepared by LPPS in near neutral 3.5 wt% NaCl electrolyte.

Z. Mao · J. Ma · J. Wang · B. Sun (✉)
State Key Laboratory of Metal Matrix Composites, Shanghai Jiaotong University, Shanghai 200240, People's Republic of China
e-mail: bdsun@sjtu.edu.cn

Z. Mao
State Key Laboratory of Explosion Science and Technology, Beijing Institute of Technology, Beijing 100081, People's Republic of China

J. Ma
Material Institute, Hebei University of Science and Technology, Shijiazhuang 050054, People's Republic of China

Introduction

Surface-modified technology through depositing protective coatings on the substrate materials (especially ceramic coatings) has been widely used in industries and aeronautic areas in recent years [1–3]. In addition, phases in coatings formed in situ, which possess the characteristics of no contamination and excellent bonding strength, have attracted researchers' interests [4, 5]. Hard ceramic phases (carbides, borides and nitrides) are formed in situ by the reactions of the injected original powder [6] and the powder with carrier gas [7] during the course of spraying.

TiN and Ti(C, N) coatings, which possess outstanding hardness, high strength and rigidity, exceptional wear resistance [8], good stability at high temperature and low friction coefficient, are utilized systematically to improve the tool life in industry [3]. Furthermore, TiB_2 also has superior properties such as high hardness (about 3200HV), high wear resistance, high corrosion resistance against molten metals and good chemical stability with a high melting point ($\sim$2,980 °C) [9]. TiB_2 coatings can become a promising candidate on tool materials, corrosion resistance and wear resistance on metallic substrates [10, 11].

At present, the TiN and Ti(C, N) coatings are mainly obtained by physical vapor deposition (PVD) [12] or chemical vapor deposition (CVD) [13]. Furthermore, plasma-assisted physical vapor deposition (PAPVD) [14] and magnetron sputtering [15] are also used to deposit Ti(C, N) coatings. Zukerman et al. [16] studied the wear

resistance of 3-μm-thick film systems consisting of Ti(C, N) single-layer and TiN/Ti(C, N) double-layer structures deposited by electron beam evaporation. They found that the plasma-nitrided layer improved the wear resistance by nearly one order of magnitude compared with untreated steel. In addition, Shenhar et al. [17] investigated microstructure and fretting behavior of hard TiN-based coatings on surgical titanium alloys. However, their applications are restricted due to the low deposition efficiency and thin coatings (below10 μm in thickness).

In order to obtain thick coatings, reactive plasma spraying (RPS) for depositing TiN coatings has been studied through the reaction between titanium powder and nitrogen plasma jets [18]. Akira Kobayashi [18], using a gas tunnel-type plasma jet, prepared 200 μm in thickness of TiN coating. In addition, Cagri Tekmen et al. [19] firstly studied on the composite coating of TiB_2 and Al_2O_3 using plasma spraying. It was found that TiB_2 and Al_2O_3 phases, dispersed finely in hypereutectic Al–Si matrix alloy, were formed in situ through the reaction of starting powder during the processing of deposition.

In this study, much work has been done on composite coatings due to their better properties than single-phase coatings. [20]. Hard ceramic coatings of Ti(C, N)–TiB_2 and TiN–TiB_2 were prepared successfully using LPPS and RPS processing, respectively. The properties of the two coatings deposited by LPPS and RPS were compared and discussed.

Experimental methods

Preparation of thermal spray powder

Commercial Ti powder (Jin Jiang Metallic powder Co. Ltd. of Shanghai, P.R. China) and B_4C powder (Sinopharm chemical reagent Co. Ltd. of Shanghai, P.R. China) were used as starting material for the deposition. Furthermore, Cr powder was added to the thermal spray powder as metallic binder for RPS. The purity of Ti powder, Cr powder, and B_4C powder are more than 99%, 99%, and 90%, respectively. In order to obtain well-proportioned powder, the thermal spray powder of Ti, Cr and B_4C for RPS was mixed by ball milling for 20 h using anhydrous ethanol as medium, then dried and sieved to obtain proper particle size (45–75 μm) for the deposition.

The powder of Ti and B_4C for LPPS was mixed by ball milling for 40 h before slurry preparation. The slurry, which consisted of disperser, bond, Ti and B_4C powder, was prepared prior to spray drying. The addition of disperser (A15) and bond (PVA) were 0.3 wt% and 1 wt% of the solid powder, respectively. The solid loading of the slurry was 40 wt%. The import and export temperatures of the drying equipment were 250 °C and 110 °C, respectively. Then, the spray drying powder was sintered in vacuum carbon tube furnace at 700 °C with the protection of argon for an hour.

Preparation of samples and coatings

Medium carbon steel (0.42–0.50 wt% C steel) with 40-mm diameter and thickness of 3 mm was used as the substrate material. The blended powder of Ti, Cr and B_4C with particle size of 45–75 μm was used as feedstock for RPS. Similarly, medium carbon steel (0.42–0.50 wt% C steel) with the dimension of 10 × 10 mm and thickness of 3 mm was used as the substrate material for LPPS. The mixed Ti and B_4C powder after spray drying and sintered was selected as top coating material. For the different thermal spraying methods, argon was selected as carrier gas. After finally polishing with 400 mesh abrasive paper, the substrates were grit blasted with alumina to get the fresh surface, ultrasonically cleaned in anhydrous ethanol, and then dried in air prior to the deposition. Buffer layer of NiCoCrAlY was selected for adjusting the miss match of thermal expansion coefficient (CTE) between the substrate and the top coating. The coating was deposited using RPS in air. The detailed spraying parameters of RPS and LPPS are shown in Tables 1 and 2, respectively.

Microstructure observation, property tests and Weibull distribution

The surface of the specimen was finely polished to avoid the effect of surface roughness before X-ray diffractometer

Table 1 RPS spraying parameters

Spraying parameters	Bond coating	Top coating
Current (A)	550	600
Power (KW)	30	35
Spraying distance (mm)	100	160
Carrier gas flow rate (L/min)	5	4
Primary gas flow rate (Ar L/h)	60	60
Secondary gas flow rate(H2 L/h)	20	40

Table 2 LPPS spraying parameters

Spraying parameters	Bond coating	Top coating
Current (A)	700	620
Voltage (V)	62	60
Spraying distance (mm)	300	300
Vacuum (mbar)	100	100
Powder feed rate (g/min)	20	24
Primary gas flow rate (Ar SLPM)	50	40
Secondary gas flow rate(H2 SLPM)	9	10

(XRD) measurement. The phase compositions of blended powder, and spray-dried, sintered powder and the coating were analyzed by XRD. The powder and cross-sectional morphologies of coatings were studied by scanning electron microscopy (SEM, JSM-6460, Japan,). Microhardness of coatings was measured by the Vickers indentor (HX-1000, Shanghai, P.R. China) with applied load of 0.1 kg and a dwell time of 15 s. The microhardness value was taken as the average value of 10 measurement points. The cross section of coatings was polished before indentation and the distance between two indentations was at least three times the diagonal to prevent stress-field effect from the nearby indentation.

Weibull distribution, which is suitable for the broad and dispersive distribution of microhardness values for brittle ceramic material, was used to analyze microhardness values of composite coatings. The Weibull distribution of two parameters is given as follows [21]:

$$F(x) = 1 - \exp\left[-\left(\frac{x}{\eta}\right)^m\right] \quad (1)$$

where $F(x)$ in Eq. 1 is the cumulative density probability function, x is the selected microhardness value, η is characteristic value and m is the Weibull modulus which reflects the dispersity of data in the distribution. The scale parameter η gives 63.2% of the cumulative density. The Eq. 1 can be transformed as follows:

$$\ln[-\ln(1 - F(x))] = m[\ln(x) - \ln(\eta)] \quad (2)$$

Therefore, a plot for $\ln[-\ln(1 - F(x))]$ versus $\ln(x)$ will be a linear relation if the Weibull modulus is suitable. The function of $F(x) = \frac{i}{n+1}$ is supposed with the data arranged in ascending order, where n in $F(x) = \frac{i}{n+1}$ is the total number of data points and i is the corresponding ordinal number [21, 22].

Electrochemical measurements

The potentiodynamic polarization curves of coatings prepared by RPS and reactive LPPS compared with bare carbon steel were studied using the CHI600C model instrument. The area of 1.0 cm^2 for the working electrode was used in the electrochemical test. Non-working surface was covered with epoxide resin. A platinum pole and Ag/AgCl electrode were used as counter and reference electrodes, respectively. To imitate the seawater environment, near neutral 3.5 wt% NaCl solution was used as electrolyte, which was static, naturally aerated and at room temperature (20 ± 5 °C). Potentiodynamic polarization tests were carried out from the initial potential of −1 V up to final potential of 3 V. The equipment with scan rate of 0.05 V/s, sample interval of 0.001 V, quiet time of 2 s, and sensitivity of 0.1 A/v were employed in the experiment.

Result and discussion

SEM morphology and composition of the powder

Figures 1 and 2 are the SEM morphologies of blended powder and spray-dried, sintered powder, respectively. It is very clear that the powder prepared by spray-drying and sintering is spherical with more uniform particle size than blended powder. The de-ionized water (solvent) in slurry with well-proportioned and dispersive powder of Ti and B_4C, is evaporated quickly during the course of spray drying. Due to large surface area of droplet and the effect of surface tension, the powder in slurry shrinks to sphericity with the evaporation of solvent.

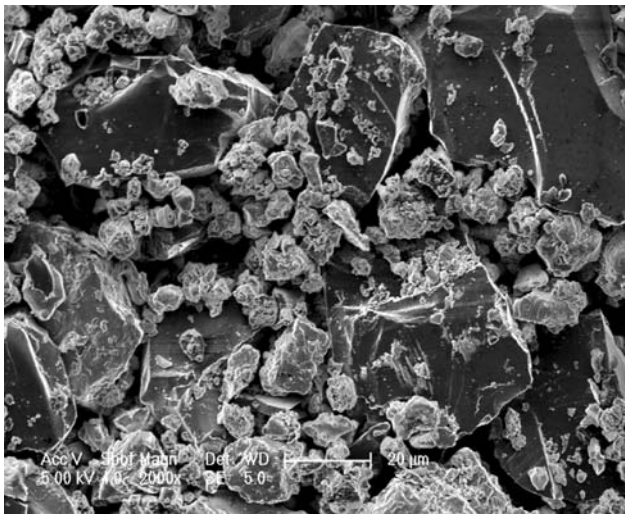

Fig. 1 The morphology of mixed powder

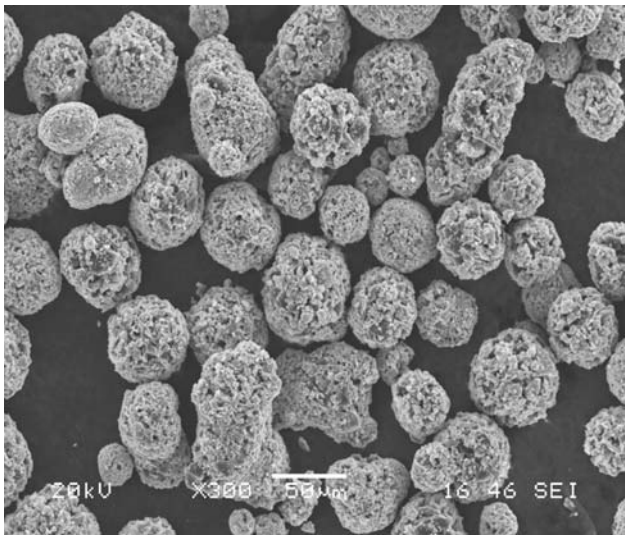

Fig. 2 The morphology of spray-dried and sintered powder

After sintering, the spray-dried powder can absorb heat, and low melting point material of A15 and PVA will volatilize to lessen the effect on the property of coatings. The bond strength of powder becomes strong due to sintering (heat treatment) of spray-dried powder. It is very helpful to the reaction of Ti and B_4C powder. Figures 3 and 4 show the XRDs of the blended powder and the spray-dried, sintered powder, respectively. The composition of the blended powder is Ti_6O, B_4C and Cr whereas the composition of the spray-dried, sintered powder is Ti_2O, B_4C, Ti_5Si_3 with a small proportion of SiO_2. The following reactions will take place during the powder preparation in air according to XRD analysis:

$$Ti(s) + 1/12O_2(g) = 1/6Ti_6O(s) \quad (I)$$

$$Ti(s) + 1/4O_2(g) = 1/2Ti_2O(s) \quad (II)$$

$$Ti_6O(s) + 12/17SiO_2(s) = 4/17Ti_5Si_3(s) + 41/17Ti_2O(s) \quad (III)$$

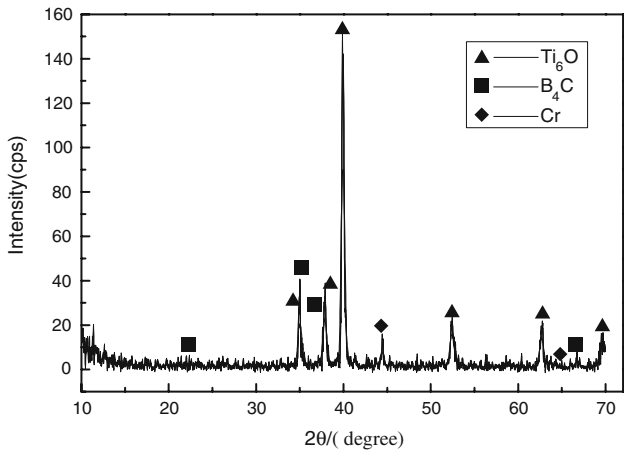

Fig. 3 XRD of mixed powder

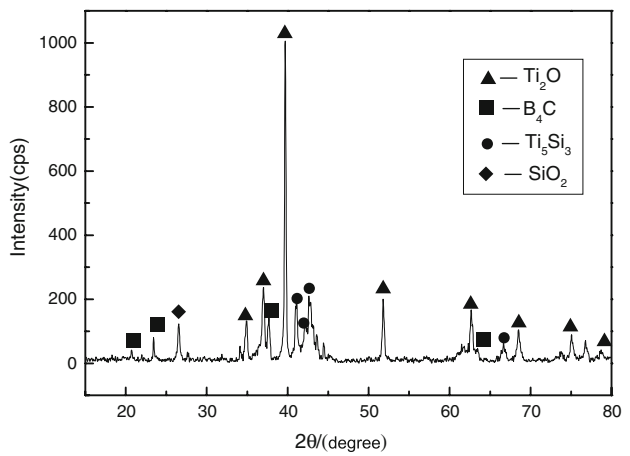

Fig. 4 XRD of spray-dried and sintered powder

The reason for appearance of Ti_6O and Ti_2O phases during preparation by thermal spray powder is that Ti powder reacts with oxygen due to the activity of Ti powder (Eqs. I and II). The undesired phase of SiO_2 is the main composition of agate ball. After ball milling and impacting drastically for a long time (40 h), the SiO_2 ingredient leaves from the agate ball and then reacts with Ti_6O in the course of ball milling, spray drying and sintering. The stability of Ti_6O is weaker and its reducibility is stronger than that of Ti_2O. Ti_6O reacts with SiO_2 to form Ti_5Si_3 and Ti_2O phases (Eq. III) during the course of spray drying due to relatively high temperature (90–110 °C) for spray drying in air. The agate ball should be responsible for the undesired production of Ti_5Si_3 and SiO_2. However, there is no SiO_2 phase in mixed powder owing to shorter ball milling time (20 h) and slower rotation speed of globe mill. The content of SiO_2 may be so little that the XRD cannot detect it ($\sim$<5 wt%).

The composition of coatings

The phase composition of coatings deposited by RPS and LPPS are shown in Figs. 5 and 6, respectively. The composition of the coating deposited by RPS consists of main phases of TiN and TiB_2, minor phases of Ti_2O_3 and TiO_2 and some unreacted original Cr powder. The TiN, Ti_2O_3 and TiO_2 phases are the results of reactions between Ti, nitrogen and oxygen due to the coating deposited in the atmosphere. The carrier gas of argon just can partially protect the powder against reaction with N_2 and O_2. Powder contact with air increases under high pressures of carrier gas.

The desired phase of TiB_2 is formed in situ during the reaction between Ti and B_4C powder. However, there is no TiC phase which should appear in the top coating

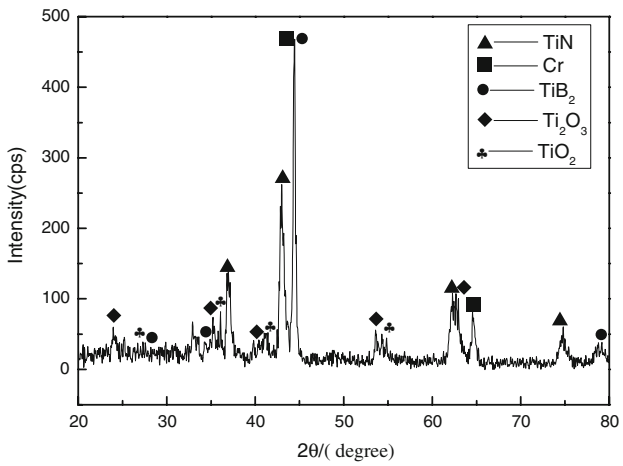

Fig. 5 XRD of RPS coating

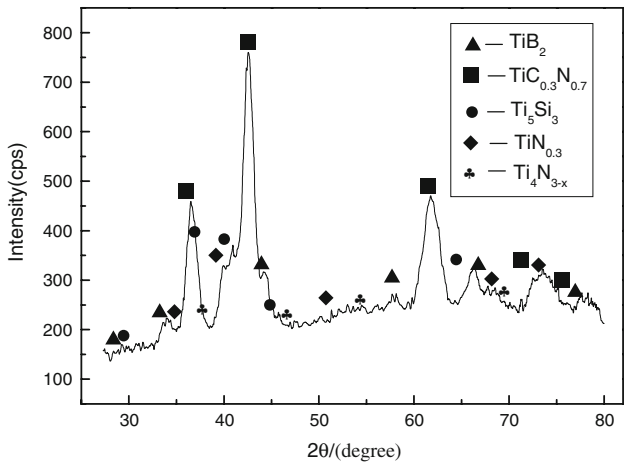

Fig. 6 XRD of LPPS coating

according to the reaction of Ti and B_4C powder. The possible reason is that the fluidity of blended powder for RPS is not good. The blended powder was separated under high pressure of carrier gas during spraying due to different density of the powder. So the contact opportunity between Ti and B_4C powder decreases and TiC phase is so little that the XRD cannot detect it ($\sim$<5 wt%).

As shown in Fig. 6, The composition of the coating deposited by reactive LPPS is main phases of $TiC_{0.3}N_{0.7}$ and TiB_2, minor phases of Ti_4N_{3-x} and $TiN_{0.3}$ and impurity of Ti_5Si_3 phase. Compared with the composition of the coating prepared using RPS, there are no titanium oxides in the coating due to relatively low air pressure for LPPS during the course of spraying. The Ti powder reacting with oxygen can be hindered in low air pressure. The feedstock with good fluidity and cohesion through spray drying and sintering reacts with each other adequately. The formation of desired phases (TiB_2 and TiC) is more due to the better reaction of sintered Ti and B_4C powder. Due to similar properties of TiC and TiN phases, they can inter-diffuse to form the $TiC_{0.3}N_{0.7}$ phase. It is similar to the TiN structure with a partial substitution of N by C [23] and has a face center cubic (fcc)-type NaCl structure.

The starting material of B_4C powder is very important for the formation of TiB_2 and $TiC_{0.3}N_{0.7}$ phases. It dissociates and provides the carbon atom during the course of spraying for desired phases in coatings. The atmosphere of deposition should be responsible for the production of TiN and Ti_4N_{3-x} phases. The ambient for the coating deposition is not absolute vacuum (100 mbar) and some residual nitrogen reacts with Ti powder. The non-equilibrium course is responsible for the complicated reactions during thermal spraying [24]. It is well known that plasma spraying, which possesses high temperature of plasma flame, can make most powder melt in a short time. Then the powder reacts quickly. The short time of coating deposition does not leave enough time to establish thermodynamic equilibrium. Several reactions can therefore take place at the same time during spraying.

Although oxidation of Ti powder prior to deposition, which is not expected to happen, the Ti_6O and Ti_2O are unstable phases and possess strong reducibility. They can react with B_4C and N_2 during spraying. Furthermore, undesired phase of Ti_5Si_3 is stable with a formation heat of −579 KJ/mol and has a high melting point (2,130 °C). Ti_5Si_3 has been extensively studied as a candidate for high-temperature structural applications due to its high melting point, low density (4.32 g/cm^3), excellent creep resistance, good strength at elevated temperature and high oxidation resistance [25, 26]. It may also have the potential application (wear-and-crack resistance) in coatings.

SEM morphology of coatings

The morphologies on the cross section of coatings deposited by RPS and reactive LPPS are shown in Figs. 7 and 8, respectively. It is found that the bond coating and top coating possess typical lamellar structure. The thermal spray powder melts at high temperature of plasma flame and then begin to react with each other. Then these droplets impact to the steel substrate and form the lamellar structure in coatings due to high velocity of plasma flame.

It is relatively thick ($\sim$350 μm) in the ceramic coating for RPS. That shows the top coating possesses good cohesion property. However, thick bond coating cannot be sucessfully deposited in view of the hand-held plasma spray gun being manually operated. Compared with the coating deposited by RPS, the structure of top coating deposited using reactive LPPS is unconsolidated and has more porosity due to lack of metallic binder. It can melt and fill in the pores in coatings during the course of

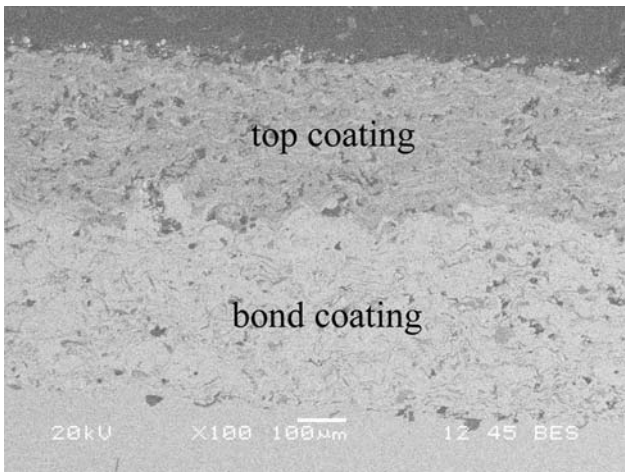

Fig. 7 SEM morphology of cross section for the coating deposited by RPS

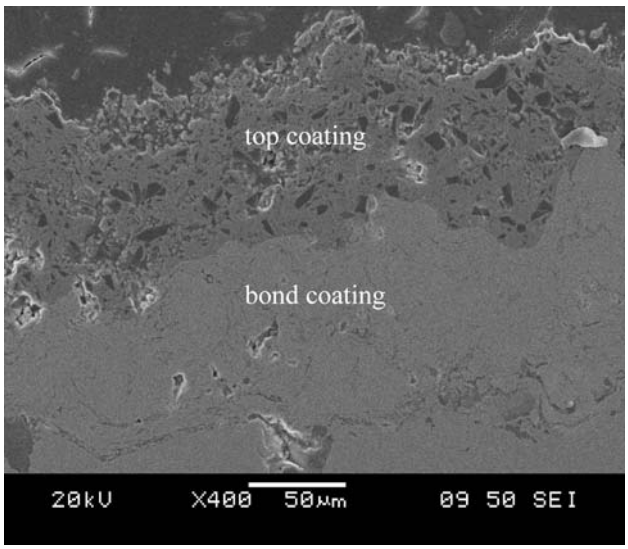

Fig. 8 SEM morphology of cross section for the coating deposited by LPPS

spraying. The metallic binder also can improve wetting property of ceramic phases in coatings. In addition, the interface of the coatings between the top coating and buffer layer adheres well.

Vickers microhardness and Weibull distribution

The mean microhardness values of 10 measurement points on the cross section are 727.5 ± 193.6 HV and 498.7 ± 98.7 HV for the coating deposited by RPS and for the coating deposited by LPPS, respectively, at 0.1 kg applied load and a dwell time of 15 s. Table 3 shows the value and standard error of Vickers microhardness. It is very evident that the average Vickers microhardness of both coatings is relatively low compared with that of ceramic coatings at the same applied load [27]. Immature technological parameters for the deposition and multiphase in the coatings should be responsible for this phenomenon. The technological parameters for deposition using powder of Ti and B_4C, which are very different from each other in property, are not very mature in RPS. In addition, several reactions taking place at the same time increases the complexity of phase composition of coatings during the course of spraying. The formation of titanium oxides decreases the content of hard phases (TiB_2, TiC and TiN) which can increase the Vickers microhardness value of coatings very much. However, the Vickers microhardness value for the coating deposited by RPS is higher than that of the coating deposited by LPPS. The less porosity and more compact structure of the coating deposited by RPS are the reasons for higher Vickers microhardness value. The structure of the coating deposited by reactive LPPS is unconsolidated due to the bad wetting property of ceramic phases in top coating.

Table 3 Vickers microhardness of coatings

Coating	Mean	Min.	Max.	SE
LPPS	498.7	356.7	662.9	33.6
RPS	727.5	417.3	1018.5	61.1

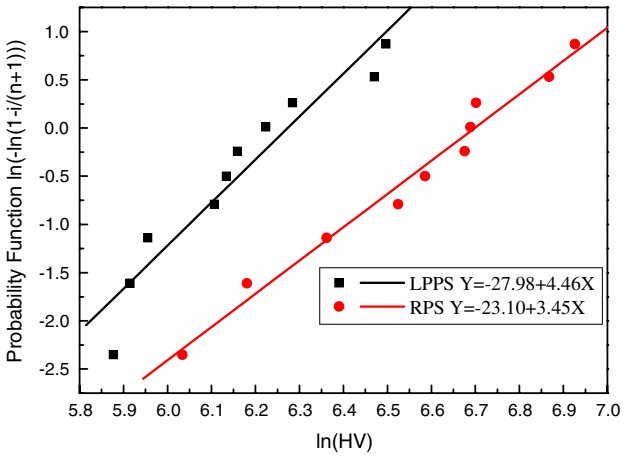

Fig. 9 Linear fitting of Weibull distribution

Table 4 Summary of the results obtained from the Weibull distribution plots

Applied load (0.1 kg)	Weibull modulus, m	SD	Hardness range in HV	ln(HV)
RPS	3.45	0.15	417.3–1018.5	6.03–6.93
LPPS	4.46	0.30	356.7–662.9	5.88–6.50

The Weibull plot of the Vickers microhardness values on the cross section at 0.1 kg applied load and their linear fit are shown in Fig. 9. The detailed information supplied by the figure is summarized in Table 4. It is obvious that both the Weibull modulus values are suitable to show a satisfactory distribution. Because the low modulus corresponds to a high variability in the microhardness measurement, the microhardness values of the coating deposited by reactive LPPS are more concentrated with higher modulus than that of the coating deposited by RPS. The hard phase distribution and the structure of coatings may be responsible for this phenomenon. For the coating deposited by RPS, there are several phases in the top coating and the Vickers microhardness values are very different from each other. The microhardness of oxides is much lower than TiN and TiB_2 phases. The indentation size can change considerably when applied load acts on the hard phase and soft phase. The values of microhardness will be much different. Contrarily, for the coating

deposited by LPPS, the phases of TiB_2 and Ti(C, N) are both relatively hard material. The difference of microhardness values between them is smaller than that of the phases in the coating deposited by RPS. Therefore, the measured microhardness values show lower variability and more uniform for the coating deposited by reactive LPPS.

Polarization curve

The anodic and cathodic polarization curves corresponding to bare carbon steel, the coatings deposited by reactive LPPS and RPS are shown in Fig. 10. Curves AB, CE and CF in the graph are cathodic polarization curves of bare carbon steel, the coating deposited by LPPS and the coating deposited by RPS, respectively. Contrarily, curves BD, EI and FI belong to anodic polarization curves. The current enhances with the increasing of potential in both these regions. This result indicates that these regions are active regions corresponding to the solution of surface material.

It is very obvious that typical passive region is found for the coating deposited by RPS and bare carbon steel. The passive potential of the coating deposited by RPS is much more positive ($\sim$0.5 V) than that of carbon steel. A protective film for the substrate is formed and the current remains same or changes a little with the increment of potential in passive region. However, compared with the other two materials, there is no apparent passive region for the coating deposited by LPPS. The current increases very slowly behind point I, which is the characteristic of passive region. It may be passive between point I and L (short region). Then it is pierced behind point L. The current behind point L begins to increase with the increment of potential. Conversely, a transition region (curve DK) appears and passive behavior (line GH) happens at relatively low potential for the bare carbon steel due to weak corrosion resistance.

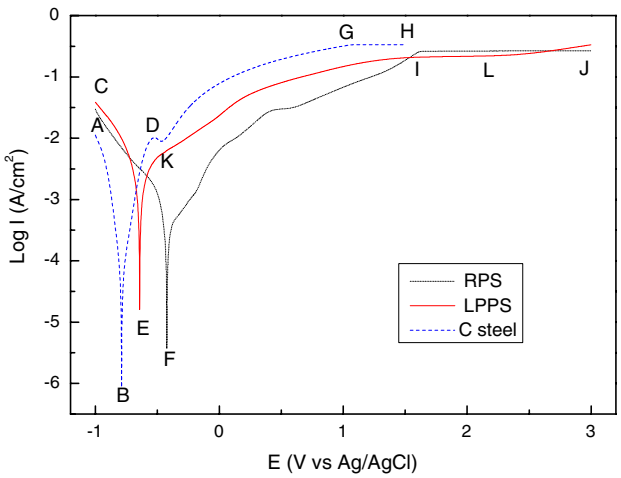

Fig. 10 Polarization curves of three materials

Although the thickness of the coating deposited by LPPS is thinner than that of the coating deposited by RPS, the corrosion potential has little relationship with the thickness of coatings due to much porosity in the top coating deposited by LPPS. The corrosion potential is more positive and the corrosion current is smaller for the coating deposited by RPS than that of the coating deposited by LPPS. This shows that the corrosion resistance of the coating deposited by RPS is better in 3.5 wt% NaCl solution. The unconsolidated structure of the coating deposited by LPPS, which provides the channel for corrosion, should be responsible for the worse anti-corrosion property. In addition, Cr as an anti-corrosion element has been widely used in the industry due to its high chemical homogeneity and high chemical reactivity [28]. Alloys containing Cr show high corrosion resistance due to formation of chromium-enriched passive films [29]. The metal Cr existed in the composition of the coating deposited by RPS can also work as the same way in the 3.5 wt% NaCl electrolyte. However, the corrosion potential of the coating deposited by LPPS is still more positive than that of bare carbon steel.

Conclusions

The coatings were deposited successfully using spray-dried and then sintered powder of Ti and B_4C for reactive LPPS and blended powder of Ti, B_4C and metallic binder Cr for RPS. The powder with good fluidity after spray drying and sintering is suitable for thermal spray. The properties of coatings were also investigated in this study. The main conclusions are as follows:

(1) The oxidation of Ti powder can be hindered in low air pressure during spraying. The coating deposited by RPS with metallic binder (Cr) is denser than that of the coating deposited by LPPS. The melting of Cr powder improves the wetting property of ceramic phases during the course of spraying.

(2) The average Vickers microhardness value on the cross section is 727.5 $\pm$ 193.6 HV for the coating deposited by RPS, which is higher than that of the coating deposited by LPPS (498.7 $\pm$ 98.7 HV) at 0.1 kg applied load. However, the latters Weibull distribution of Vickers microhardness values with higher Weibull modulus value is more concentrated than that of the coating deposited by RPS.

(3) Thick coatings can improve the anti-corrosion property of bare carbon steel obviously. The coating deposited by RPS with longer passive region, more positive corrosion potential and smaller corrosion current possesses a better anti-corrosion property in

3.5 wt% NaCl electrolyte. However, the corrosion mechanism should be investigated more in the future.

Acknowledgements This study was financially supported by the Opening fund Program of China (No. KFJJ07-2). The authors are grateful to Mr. H. Ji and Mr. X. M Zhu for depositing of coatings, and the XRD analysis by Mr. H. B. Han for in the instrumental analysis centre of Shanghai Jiaotong University. The authors are also thankful for the hard work of editors and reviewers on this article.

References

1. Tu JP, Rong W, Guo SY, Yang YZ (2003) Wear 255:832
2. Cairo CAA, Florian M, Graca MLA, Bressiani JC (2003) Mater Sci Eng A 358:298
3. Bull SJ, Bhat DG, Staia MH (2003) Surf Coat Technol 163–164:499
4. Singh A, Dahotre NB (2004) J Mater Sci 39:4553. doi: 10.1023/B:JMSC.0000034149.95969.bc
5. Anal A, Bandyopadhyay TK, Das K (2006) J Mater Process Technol 172:70
6. Liu HY, Huang JH, Yin CF et al (2007) Ceram Int 33:827
7. Xiao L, Yan D, He J et al (2007) Appl Surf Sci 253:7535
8. Chavanes A, Pauty E, Woydt M (2004) Wear 256:547
9. Kang YS, Kang SH, Kim DJ (2005) J Mater Sci 40:4153. doi: 10.1007/s10853-005-4153-3
10. Wang XB, Shun HL, Li CG et al (2006) Surf Coat Technol 201:2500
11. Xu J, Liu WJ (2006) Wear 260:486
12. Stoiber M, Panzenbőck M, Mitterer C, Lugmair C (2001) Surf Coat Technol 142–144:117
13. Liu Z-J, Leicht P, Liu Y-X, Liu Z-K (2006) Surf Coat Technol 201:2818
14. Puchi-Cabrera ES, Staia MH, Quinto DT et al (2007) Int J Fatigue 29:471
15. Polcar T, Kubart T, Nova′k R et al (2005) Surf Coat Technol 193:192
16. Zukerman I, Raveh A, Kalman H et al (2007) Wear 263:1249
17. Shenhar A, Gotman I, Radin S et al (2000) Surf Coat Technol 126:210
18. Kobayashi A (2000) Surf Coat Technol 132:152
19. Tekmen C, Tsunekawa Y, Okumiya M (2008) Surf Coat Technol 202:4170
20. Wen G, Li SB, Zhang BS, Guo ZX (2001) Acta Mater 49:1463
21. Zhou H, Li F, He B et al (2007) Surf Coat Technol 201:7360
22. Lima RS, Kucuk A, Berndt CC (2002) Mater Sci Eng A 327:224
23. Levi G, Kaplan WD, Bamberger M (1998) Mater Lett 35:344
24. Mao Z, Ma J, Wang J, Sun B (2009) Appl Surf Sci 255:3784
25. Stoloff NS (1999) Mater Sci Eng A 261:169
26. Yeh CL, Wang HJ, Chen WH (2008) J Alloy Compd 450:200
27. Feng W, Yan D, He J et al (2005) Appl Surf Sci 243:204
28. Hashimoto K, Osada K, Masumoto T, Shimodaira S (1976) Corros Sci 16:71
29. Habazaki H, Ukai H, Izumiya K, Hashimoto K (2001) Mater Sci Eng A 318:77